ELSEVIER

Temporal Mixture Analysis of Arctic Sea Ice Imagery: A New Approach for Monitoring Environmental Change

Joseph M. Piwowar, Derek R. Peddle,*† and Ellsworth F. LeDrew**

In this paper, we introduce the idea of temporal mixture analysis (TMA) for analyzing long sequences of hypertemporal remote sensing imagery. The basis of this approach is spectral mixture analysis, which we adapt from the spectral domain to the time domain. The TMA procedure is demonstrated by applying it to a 9-year record of scanning multichannel microwave radiometer sea ice concentrations in the Northern Hemisphere. We find that end-member fraction images provide a unique summary of spatial arrangements and temporal characteristics of the mapped phenomenon during a specific period and can be used to characterize climatic normals. A key distinction that differentiates temporal mixture imagery from similar images derived through more traditional means is that the data presented are derived from the temporal *characteristics of the analyzed phenomenon and not the* type *of feature present. ©Elsevier Science Inc., 1998*

INTRODUCTION

Remote sensing has played a particularly prominent role in the monitoring of climate change; it is the only source of data with which we can view the entire planet and monitor the change in the nature of the surface of the planet through time, in a consistent, integrated, synoptic, and numerical manner (Davis et al., 1991; LeDrew, 1992). Global observations of the earth by satellite sensors are required simply because no other approach permits measurements to be made at the required spatial and temporal resolutions.

Routine, repetitive, and continuous observations of Earth's surface from operational remote sensing systems began in the early 1970s with the launch of the Landsat-1 and Nimbus-5 satellites. The Landsat series of platforms, and other more recent systems (e.g., NOAA, SPOT, IRS-1), carry optical sensors that continue to supply us with valuable Earth resource information, primarily over subpolar land surfaces. Similarly, the primary sensors aboard the Nimbus-5, Nimbus-7, and Defense Meteorological Satellite Program (DMSP) satellite sequence have allowed polar scientists to amass a continuous record (except for a 2-year gap between Nimbus 5 and Nimbus 7) of Earth's Arctic and Antarctic snow and ice covers. Thus we have a remote sensing data archive that is quickly approaching the 30-year mark from which we may be able to determine a climate signal.

Although satellite remote sensing has long been advocated for monitoring surface processes through time, remarkably little progress has been made in quantitative spatial-temporal analysis of multitemporal imagery (Davis et al., 1991). There is a need to place the compilation of data sets from past records on an equal priority with the development of new observing systems. We need to support the recovery and reprocessing of existing global change data sets and ensure the long-term continuity of future Earth-observing systems (UCAR, 1990). We must create techniques that highlight the space-time relations in data rather than simply displaying voluminous quantities of output. In particular, new image analysis techniques are required to help find expected trends and to discover unexpected temporal relations in long sequences of remotely sensed imagery. This is the domain of *hypertemporal* image analysis.

* Waterloo Laboratory for Earth Observations, Department of Geography, University of Waterloo, Waterloo, Ontario, Canada

† Now with the Department of Geography, University of Lethbridge, Lethbridge, Alberta, T1K 3M4, Canada

Address correspondence to Joseph M. Piwowar, University of Waterloo, Waterloo, Ontario, N2L 3G1, Canada. E-mail:piwowar@watleo.uwaterloo.ca

Received 4 October 1996; revised 9 June 1997.

REMOTE SENS. ENVIRON. 63:195–207 (1998)

655 Avenue of the Americas, New York, NY 10010

0034-4257/98/$19.00
PII S0034-4257(97)00105-3

Hypertemporal image analysis is still in its infancy. Published reports describing techniques for the quantification of variability and change in remotely sensed image sequences are absent. New tools must be developed and tested to determine their applicability in climate change studies. In this paper, we describe the extension of the hyper*spectral* image processing technique of spectral mixture analysis (SMA) into the temporal domain—a technique that we call *temporal mixture analysis* (TMA). We show how TMA can be used to define long-term normals in hypertemporal image data sets. This is illustrated through the application of TMA to a 9-year record of monthly Arctic sea ice concentration images—108 images in all—derived from data collected by the scanning multichannel microwave radiometer (SMMR) carried aboard the Nimbus-7 platform.

ARCTIC SEA ICE AND CLIMATE CHANGE

Climatologists have been concerned for some time about the possible climatic ramifications of increased atmospheric concentrations of anthropogenically produced greenhouse gases. Many general circulation model experiments show amplified warming in the polar regions as the strongest response to enhanced atmospheric greenhouse gas concentrations. In light of this, a spatially coherent pattern of high-latitude temperature trends has been speculated to be an early indicator of climatic change. The sensitivity of sea ice to the temperature of the overlying air implies that observed trends in Arctic ice conditions may also indicate general climatic changes.

Remote sensing in the passive microwave part of the electromagnetic spectrum is particularly relevant for polar applications because microwaves are capable of penetrating the atmosphere under virtually all conditions (of particular significance during the frequent and extended periods of cloudiness in the Arctic) and microwave remote sensing systems are not dependent on the sun as a source of illumination (an important consideration during the long polar night of winter). A historical record of Arctic imagery from orbiting passive microwave sensors starting from 1972 provides us with an excellent data source for studying climate change and variability.

In this study, 9 years of sea ice concentration data derived from SMMR imagery were analyzed. The SMMR was a 10-channel instrument that operated on the Nimbus-7 spacecraft between November 1978 and August 1987. It measured emitted Earth radiation at five dual-polarized frequencies between 6.63 and 37.0 GHz in the microwave part of the electromagnetic spectrum. The SMMR data used in this study are derived from those published on the Nimbus-7 SMMR Radiances and Sea Ice Concentrations CD-ROM (volume 7) produced by the NASA Oceans and Ice Branch at the Goddard Space Flight Center and distributed by the National Snow and Ice Data Center in Boulder, CO. Ice concentration is the percentage of a given area of ocean (a pixel, in this analysis) that is covered by ice and is a measure of the amount of open water within the ice margins. Even in the middle of winter, concentrations of less than 90% can be found in the middle of the Arctic pack ice largely as a result of open leads and polynyas.

Although passive microwave imagery was collected from orbiting satellites for 4 years before SMMR (Nimbus-5 electrically scanning microwave radiometer) and for all of the years since then (DMSP special sensor microwave/imager), the analyses presented herein are restricted to the SMMR data set to prevent the introduction of errors arising from the processing of images from more than one sensor. Although the 9-year SMMR data record is too short to make any definitive statements about climate changes from the results, it is an excellent test bed for developing new interpretation strategies. We use the SMMR data to show how temporal end members can be generated and applied to define long-term normals and departures from those normals.

HYPERTEMPORAL IMAGE ANALYSIS DATA REQUIREMENTS

When preparing a data set for hypertemporal image analysis, three requirements must be met: (1) the data must be univariate at each temporal instance; (2) precise coregistration of each time slice must be guaranteed; and (3) there must also be some normalization of the data values between slices before beginning any analysis. The first requirement was satisfied by using processed ice concentration images instead of radiance data directly from the 10 SMMR channels. If we ignored this requirement and included several spectral channels for each time period in our analyses, it would be difficult to determine whether any patterns observed in the image series were temporal or spectral in origin.

The second hypertemporal specification is the requirement for precise coregistration of each data layer. In conventional analyses of optical remote sensing imagery, image registration is usually accomplished through a nonlinear "warping" of the image data to spatially align them with either a geographic grid or another image's coordinate system. Random geometric distortions in the source imagery and the nonlinear nature of the image warping process cannot guarantee that every cell in the registered data set will have an equally accurate registration. In contrast, SMMR orbital swath imagery is mapped to a predefined polar grid in accord with a "drop-in-the-bucket" method in which a grid cell that is covered by two or more SMMR pixels (owing to overlapping swaths poleward of 72°) is assigned the value of the last pixel to cross it—not the average of all the observations from that day. The drop-in-the-bucket approach does ensure precise image-to-image registration because the image data are never warped.

The third requirement of radiometric (or similar) consistency between each image stems from the need to ac-

count for differences in pixel values due to effects such as atmospheric attenuation, changes in target illumination, and sensor decay. This is typically accomplished through a radiometric calibration or normalization of each layer. Interscene radiometric variations may also be accounted for in the use of derived products based on spectral channel ratios such as normalized difference vegetation index (NDVI) images of optical data. This is also the case for ice concentration scenes from passive microwave values. Radiometric artifacts due to extreme atmospheric events, such as very heavy rainfall, or signal variations arising from sensor decay or both, may remain in the data, however, even after ratioing or radiometric calibration (Eastman and Fulk, 1993). Such artifacts are not expected to be present in the SMMR data, because the images have been corrected for sensor drift and processed with a "weather filter" (Gloersen et al., 1993). In addition, the processing of the SMMR images into monthly averages serves to minimize fluctuations that may result from atmospheric and other short-term effects (Comiso, 1986).

SPECTRAL MIXTURE ANALYSIS

Although the spatial resolution of orbital sensors has increased by a factor of eight over the past 20 years—a feat that is expected to be repeated in the next 5 years—a large proportion of remotely sensed data are spectrally mixed because the scales of spatial variation of natural phenomena are often smaller than the spatial resolutions of sensors. Thus a fundamental, yet often overlooked, concept is that each single radiance value recorded by a sensor in image acquisition actually contains contributions from several individual surface components. SMA is a procedure that attempts to extract the fractional radiance components from the pixels in an image.

The primary objective of SMA is the isolation of the main spectral contributions in each pixel. Although the spectra in question have traditionally been derived from radiance measurements at various wavelength bands in the electromagnetic spectrum, Adams et al. (1993) suggest that the technique is extensible to any physical attribute that can be measured at each pixel, such as net radiation, radar backscatter, or even elevation. In this paper, the application of SMA is in the temporal domain.

The concept of spectral mixture analysis was introduced by Horwitz et al. (1971) and later became more popular as a tool for geologic mapping (Adams et al., 1989; Hoffbeck and Landgrebe, 1993; Sabol et al., 1990). It has also been successfully used in such diverse applications as forestry (Cross et al., 1991; Hall et al., 1995; Peddle et al., 1997; Unger and Bryant, 1981), ecological modelling (Ustin et al., 1993), and coral reef abundance (Peddle et al., 1995). Although it has been used extensively for the analysis of hyperspectral data from imaging spectrometers where conventional image analysis techniques have been shown to be inadequate (Adams et al., 1993; Boardman, 1989), it has also been used with Landsat thematic mapper imagery (Gong et al., 1991) and for the integration of diverse data sets (Gillespie et al., 1990).

SMA is commonly used to identify the spectral contributions of subcomponents within a remote sensor's instantaneous field of view. Adams et al. (1993) define this algorithmically as

$$DN_p=(EM_1{}^*F_1)+(EM_2{}^*F_2)+ \ldots +(EM_n{}^*F_n)+\varepsilon, \quad (1)$$

where:

DN_p is the pixel's digital number
EM_i is the spectrum of the ith endmember (where there are n endmembers in the model)
F_i is the fractional contribution of the ith endmember
ε is any residual contribution not accounted for by the endmember set

From Eq. (1), we observe that the SMA procedure is driven by summing the fractional contributions of a set of spectral *end members*. End members represent the most extreme, or "pure," spectra for a given feature in the image. Finding pure endmembers in multidimensional image data (known as *image* end members) can be difficult, because a large enough pure target must be known to exist within the scene. Analysts may also define *reference* end members from field spectrometer measurements or from external data sources such as spectral libraries; selected end members may also be generated by using physical models (Hall et al., 1995; Peddle et al., 1997).

In practice, images entered into a SMA procedure are assumed to contain spectrally mixed data: they are *unmixed* to find the fractional contribution of each of its end members. This produces one *fraction image* for each end member and a root-mean-square (RMS) *error image* containing any residual spectral components not accounted for by the end-member set. Referring to Eq. (1), we are given *DN* and specify *EM*, so the equation is inverted to solve for *F*. For a more detailed description of this process, see Adams et al. (1993), who provide an excellent introduction to the concepts behind spectral mixture analysis.

TEMPORAL MIXTURE ANALYSIS

In spectral mixture analysis, fractional images are created that describe how much each pixel in the scene is related to the reference spectra (end members) where the reference spectra are defined as radiometrically pure features. In this study, the SMA technique is extended to analyze temporal spectra of SMMR sea ice concentrations to determine if end-member fractions can be created from temporally pure features (e.g., "no change" and "seasonal change"). If the SMA technique is applied to an annual summary of the SMMR data, it was expected that an overview of the temporal characteristics of Arctic sea ice processes could be derived and subsequently used as a proxy of the long-term normal. To facilitate this investi-

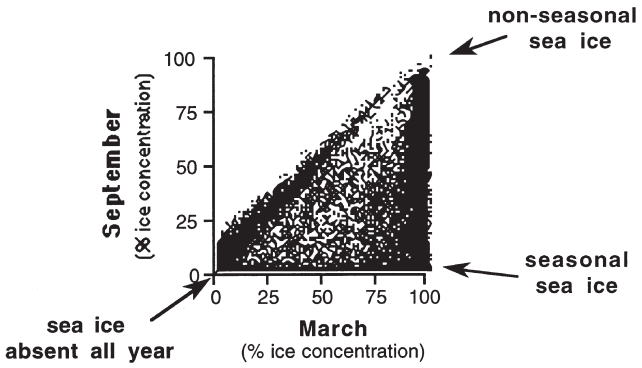

Figure 1. Basic end-member definitions. Plotted values are the 9-year mean sea ice concentrations between March and September. The presence of pixels that appear to have higher concentrations in September than in March are due to land and atmospheric contamination of the SMMR signal in subpolar regions.

gation, the 108 monthly images in the source SMMR data set were averaged by month to create a 12-month summary of mean sea ice concentrations (e.g., the nine January images were averaged to create the January summary, etc.). This 12-image sequence was the data set analyzed for temporal mixtures.

From the outset, SMA modelers are faced with the problem, "What end members should be included in the (initial) model?" End-member specification is equally important in TMA. In the present study, the initial end-member set was derived from basic principles by using a scatter plot between the known maximum and minimum temporal bands of sea ice concentration: March and September (Fig. 1).* The triangular shape of the data cloud suggests a need for three temporal end members: (1) nonseasonal sea ice (100% concentration in both March and September), (2) seasonal sea ice (100% concentration in March and ice free in September), and (3) open ocean (sea ice absent all year). All other temporal relations between March and September ice concentrations are definable as linear mixtures of these three end members.

The purest form of nonseasonal sea ice can be intuitively defined as 100% concentration (i.e., "no change") for each month of the year. Because it was unlikely that such a pure sample existed in the SMMR data the nonseasonal sea ice end member was defined manually as a reference end member. Similarly, the open ocean end member could be set to be 0% ice concentration (i.e., "no change") for each of the 12 months. Note that, because these two end members are direct linear combinations of each other, they would be treated as replicate end members in the mixing model. This was verified by running the unmixing procedure with three end-member inputs: nonseasonal sea ice, seasonal sea ice, and open ocean. The resulting fraction images revealed that the ocean areas were included in the nonseasonal sea ice image as fractions of 0.0 nonseasonal sea ice. Because these areas had already been accounted for, the water areas in the ocean fraction image were flagged as fraction underflows less than 0.0. Consequently, it was not necessary (or desirable) to include both "no change" end members in the mixing model, so only the nonseasonal sea ice end member was included for further analysis.

The exact nature of the temporal spectrum of the seasonal sea ice end member was not known, except that it was presumed to have maximum concentration in March and minimum values in September. Consequently, this end member was derived from the image data by finding those areas that met these criteria and sampling the temporal spectra from points within these regions (Fig. 2).

A total of six spectra were extracted from the image data to define the seasonal sea ice end member. This created a new issue: exactly how should these spectra be combined to form the end member? By definition, end members should be the "purest" spectra in the image. "Pure" spectra, in the context of spectral mixture analysis, means that, at any spectral interval, there should not be any other spectral samples with more extreme values than that of the end member. This concept was embodied in a *purification formula* developed in this study to derive pure end-member spectra from a sampled set of image spectra:

$$EM_i = \begin{cases} \text{MAX}_i \text{ if } \text{MEAN}_i > \text{MEDIAN}_I \\ \text{MIN}_i \text{ if } \text{MEAN}_i < \text{MEDIAN}_I \end{cases} \quad (2)$$

where:

EM_i is the endmember spectral value for the ith spectral interval (where i is represented by *month* in the present context)
MAX_i is the maximum of all sampled spectral values at the ith spectral interval
MIN_i is the minimum of all sampled spectral values at the ith spectral interval
MEAN_i is the mean of all sampled spectral values at the ith spectral interval
MEDIAN_I is the median of all sampled spectral values at all spectral intervals

From Eq. (2), we see that, if the position of the spectral samples for a given interval were above the middle (median) of the overall spectra, then the end member would be assigned the maximum sampled spectral value. If the position of the spectral samples were low, relative to the midpoint of the overall series, then the end member would be assigned the minimum spectral value. As an example, consider the three temporal spectra shown in Table 1. The median ice concentration from all three spectra is 90. In June, the mean ice concentration value

*Owing to the thermal inertia of sea ice, the sea ice seasons lag behind atmospheric seasons by 2 or 3 months. Thus the winter maxima ice concentrations are usually observed in late February or March, and the summer minima are in September.

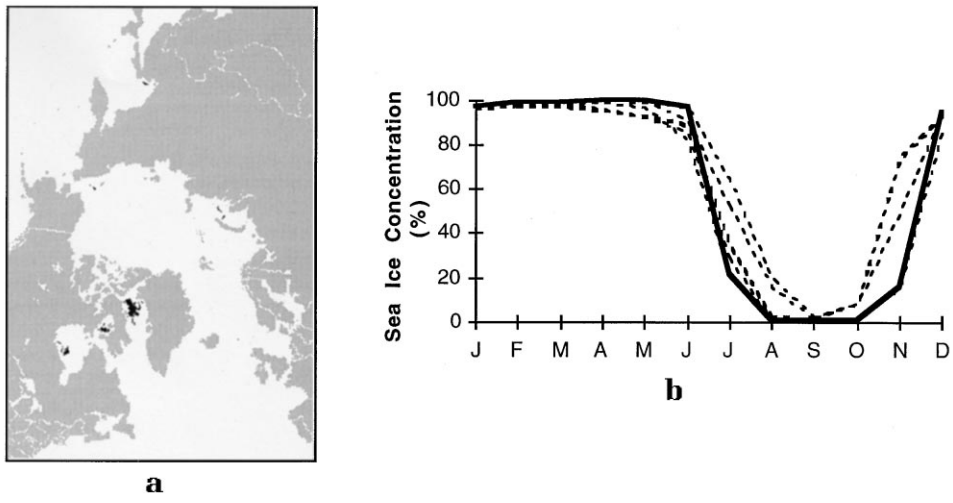

Figure 2. First seasonal end-member definition. (a) Highlighted pixels indicate locations where the 9-year mean March ice concentrations are greater than 97% and the 9-year mean September concentrations are less than 3%. (b) Temporal spectra sampled from the highlighted regions. The heavy line is the "purified" end member derived from these spectra.

(87) is less than the overall median (90), so the end-member component for this month is set to the minimum of the sampled June values (82). Likewise, the mean December value (92) is greater than the median (90), so the end member is set to the maximum December value (95).

TWO END-MEMBER MODELING

The two end members—nonseasonal ice and seasonal sea ice—were used to extract their relative fractions from the SMMR data by using the PCI image analysis system (PCI, 1996). Fraction images for nonseasonal ice and seasonal sea ice, as well as the RMS error image, are shown in Figure 3. From a spatial perspective, the nonseasonal and seasonal ice fraction images fit the known distribution of these ice types very well. The highest nonseasonal ice fractions are found in the central Arctic Ocean, above the Canadian Archipelago (see Fig. 9 for the location of Arctic place names mentioned in this article). This is the location of the oldest and slowest drifting ice in the Arctic. The nonseasonal ice fractions in the bulk of the Arctic Basin are all greater than 0.7. Toward the periphery, the nonseasonal fractions drop off rapidly but are complemented by corresponding increases in seasonal ice fractions. As expected, the seasonal sea ice zone defined by the fraction image forms a circular ring generally within the 60°–70° N latitude band. Seasonal sea ice fractions of more than 0.9 are found throughout this band but have the widest extent in Hudson and Baffin Bays and in the Barents, Kara, and Chukchi Seas. These regions have very high ice concentrations in March and become ice free in September.

In the RMS error image, lighter tones show areas where the model has a good fit with the data. These regions can be seen generally in the nonseasonal sea ice zone, in the Chukchi and Kara Seas, and in Baffin Bay. Interestingly, some areas, such as in Hudson Bay and in the Barents Sea, that showed very high seasonal sea ice fractions also had moderate errors on the error image, indicating the possible presence of additional temporal signals in these regions. Further, the presence of very high errors in areas where the sea ice fractions from the modeled seasonal end member were low, such as in the Be-

Table 1. Example Data for End Member Purification

Month	*Spectra 1*	*Spectra 2*	*Spectra 3*	*Max*	*Mean*	*Min*	*Purified End Member*
J	97	96	97	97	97	96	97
F	98	97	99	99	98	97	99
M	98	98	99	99	98	98	99
A	95	99	100	100	98	95	100
M	92	97	100	100	96	92	100
J	88	82	91	91	87	82	82
J	35	22	53	53	37	22	22
A	2	1	16	16	6	1	1
S	1	2	2	2	2	1	1
O	1	8	8	8	6	1	1
N	16	50	73	73	46	16	16
D	87	95	93	95	92	87	95

Median=90

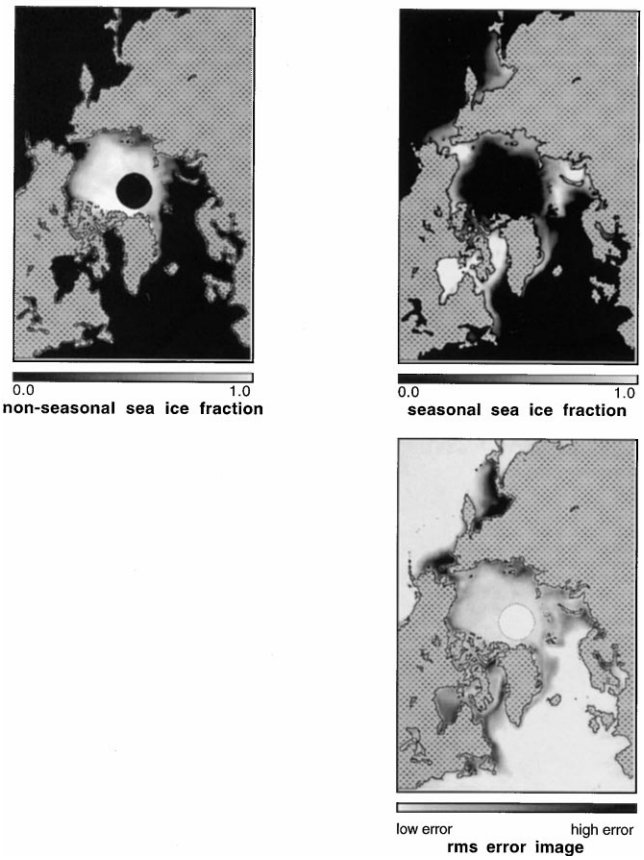

Figure 3. Fraction and error images for the two end-member model. The "hole" over the North Pole represents missing data: the SMMR orbit precluded the collection of imagery north of 84°.

ring Sea and the Sea of Okhotsk, suggests that the TMA model could be further refined.

This seasonal sea ice end member was created by using a purification formula, defined in Eq. (2). The corresponding fraction overflow image did not show any areas that had a purer signature. This result, in combination with the general agreement of the seasonal sea ice fraction distribution with the known locations of these ice types, suggests that the purification formula is an appropriate method of defining an end member from a selection of image-based spectra.

FOUR END-MEMBER MODELING

The RMS error image from the two end-member model highlighted areas that were not well described by that model, suggesting the need for additional end members. With the use of the nonseasonal and seasonal sea ice endmembers (as defined earlier) as a base, new seasonal ice end members were added to the model by using an empirical approach. The spectrum for each end member was defined from a purified selection of temporal spectra extracted at locations with high RMS errors. After two new end members were added to the original two spectra, it was noted that:

1. the RMS errors from the four end-member model were generally low over the entire Arctic sea ice zone (except for a few small pockets of moderate errors);
2. when additional end members (beyond these four) were tested, the size of the regions that were well fit by each additional end member (as characterized by high fractional components) was not significant; and
3. additional end members tended to be simple refinements of previous end members in the model, high-lighting a particular variation of the overall end-member spectrum.

Because none of the additional end members tested (beyond the four specified) defined unique spectral or spatial characteristics (i.e., they were all subsets of existing end members in the model), the analysis converged on the four end-member set. For each of the four modeled end members, corresponding spectral plots and fraction images are shown in Figure 4.

The nonseasonal sea ice fraction for the four end-member model is nearly identical with that extracted with the two end-member model. Given that the area covered matches the region known to have a permanent sea ice cover and that exactly the same end-member spectrum was used in both cases, this two and four end-member similarity is a correct and expected result. This match helps to further validate the TMA procedure because the fraction images correspond to a known ice distribution. From this, we can assume that the model is capable of correctly identifying regions on the basis of their temporal properties.

The first seasonal end member highlights some of the most dramatic seasonality in the Arctic sea ice zone. The spectral curve exhibits near total ice concentration from November through May. There is a steady opening up of the ice cover in June and July until August when it is ice free. Ice rapidly forms again in the fall so that, by November, complete coverage is again realized.

Spatially, the fraction image shows regions exhibiting these characteristics as most of the peripheral seas ringing the nonseasonal sea ice of the central Arctic Ocean. The spatial and spectral position of this end member directly adjacent to the nonseasonal ice reveals an interesting characteristic of the Arctic sea ice cover: regions of only partial clearing of ice during the Arctic summer are rare; that is, the need for an end-member definition spectrally halfway between nonseasonal ice and the first seasonal ice is not evident from the data. Previous analyses of the SMMR imagery have shown that, in the central Arctic, sea ice concentration summer minima do not get much lower than about 75% (Piwowar and LeDrew, 1996); these regions are accounted for by the nonseasonal end member defined here. If there were areas for which

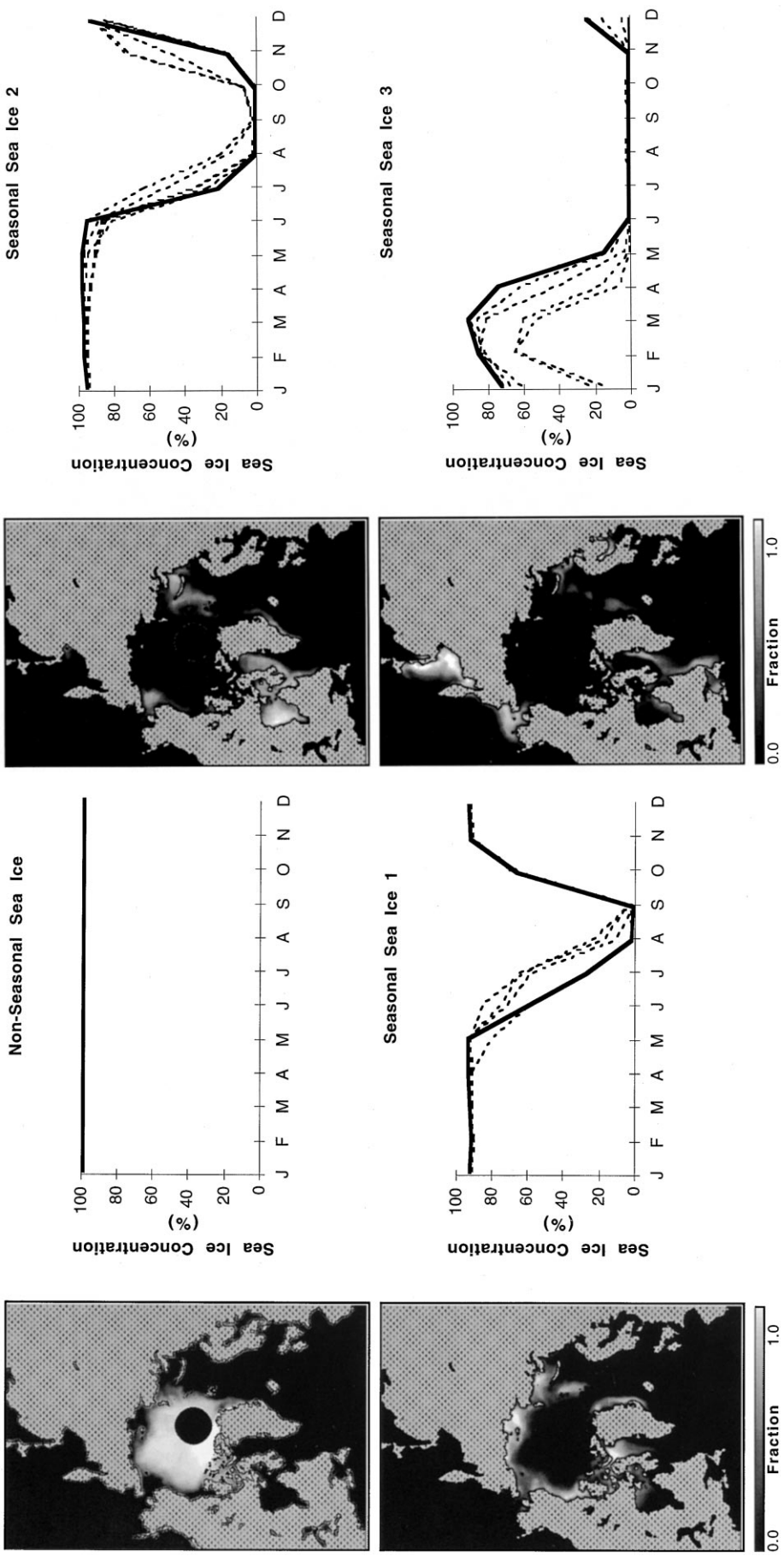

Figure 4. Fraction images and end-member spectra for four end-member model. Dotted lines are sampled image spectra; the heavy line is the "purified" spectra used in the end member.

the summer minimum ice concentration was between 10–60%, they would have been highlighted as fraction overflows in the first seasonal fraction image or as having high residuals in the RMS error image or both, but neither occurred. Consequently, although some seasonal fluctuation may be expected in "nonseasonal" sea ice, when an area opens up to below 60–70% ice concentration, it will almost certainly clear completely for at least a 1-month period during the summer.

The second seasonal sea ice fraction image was derived from the same seasonal end-member definition that was used in the two end-member model (100% ice coverage in March and 0% in September). Regions with these temporal characteristics have almost total ice coverage from December to June, undergo a rapid clearing in June and July, remain ice free for August and September, and quickly freeze to high ice concentrations in October and November. The fraction image identifies these characteristics to be primarily located in Hudson and Baffin Bays, and in the Chukchi, Kara, and Barents Seas. Each of these regions is a location of relatively limited ice movement throughout the year (although this is not unique to these regions), possibly due to shallow bathymetry and to the restrictive presence of landmasses that partially segregate these areas from the main Arctic drift streams. This limited ice motion could promote the quick ice formation and ice stagnation observed in the end-member spectrum. In addition, for Hudson Bay, the region with the closest match to the second seasonal end-member, its location deep within the North American landmass gives it a continental climate with cold, dry winters (Gloersen et al., 1993). The persistence of the ice cover in Hudson Bay may be further enhanced through the freshening of the surface water layers by the major river systems that empty there.

The third seasonal sea ice end member characterizes much of the ice in the more southerly extents of the seasonal sea ice zone: in the Sea of Okhotsk and in parts of the Bering and Labrador Seas. These areas are free of ice for almost as long as they have a measurable ice cover. After reaching a peak concentration of about 80–90% in February or March, the ice coverage decreases steadily so that by June the region is ice free. It remains devoid of ice for 5 months until November, when the coverage begins to increase again.

The RMS error image generally reveals a well-fitting model with low errors, particularly in the nonseasonal sea ice zone, with some slightly higher errors observable in the areas covered by the seasonal end members (Figure 5). Thus we conclude that there are four basic temporal models that can be used to describe the annual cycle of sea ice concentration for any point in the Arctic (based on the data used in this study). Three of these models reveal different aspects of the seasonality of the ice cover, and the fourth is used to model nonseasonal sea ice. The four end-member model developed here can be a simple, yet effective replacement for the overly simplified ice descriptions used in some general circulation models.

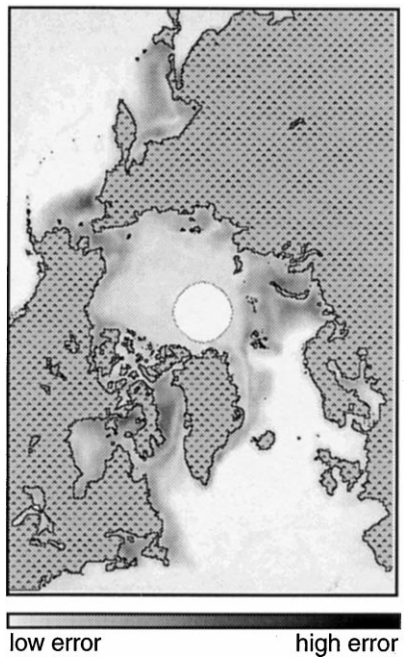

Figure 5. Four end-member model error image.

TEMPORAL MIXTURE IMAGES

Each of the four end-member fraction images shows a representation of the spatial distribution of a particular temporal signature that was unmixed from the annual time series. A composite summary of the temporal characteristics of Arctic sea ice can be obtained by remixing each end member in a red-green-blue color space, as in Figure 6. This image was created by portraying the first seasonal fraction image in red, the second in green, and the third in blue. The nonseasonal sea ice fraction was added equally to each color component so that it appears white in the color output. The intensity of each end member's color is directly related to the fractional contribution that each end member makes to the temporal characteristics of Arctic sea ice. Areas of "pure" red, green, or blue indicate regions where the monthly variability of the sea ice concentrations closely follows the corresponding end-member spectrum. Color mixtures are present where there are temporal mixtures of ice characteristics. For example, the pure green regions in Hudson Bay or blue areas of the Sea of Okhotsk point to the high fractions of the ice in these regions with temporal characteristics closely resembling the second and third seasonal end members, respectively. The pink tones in the East Siberian Sea suggest that this region is dominated by a mixture of seasonal sea ice 1 (red) and nonseasonal sea ice (white) characteristics. Similar color mixtures

are evident in the different end-member transition regions where no single temporal characteristic is dominant.

A key distinction between temporal mixture imagery and similar images derived through other means (e.g., principal components analysis or image classification) is that the data presented are derived from the *temporal characteristics* of the ice distribution and not the *type* of ice present. Thus, a region that is highlighted by the nonseasonal ice fraction is not necessarily dominated by multiyear ice. It is, however, dominated by ice whose month-to-month variation is closely aligned with the temporal spectrum defined for this end member.

TMA AS A TOOL FOR CHANGE ANALYSIS

Temporal mixture images provide a unique summary of the spatial arrangement of the temporal characteristics of the mapped phenomenon during a specific period. In the preceding section, for example, a temporal mixture image was created to describe the annual spectra of Arctic sea ice concentrations averaged over the 9-year SMMR life span. End members developed for a particular feature set should be directly applicable to other realizations of the same features so that spectral variations between them will be highlighted in their fraction and error images (Adams et al., 1993). If they were applied to annual subsets of the SMMR data, it was expected that the fractional images could serve as a historical record or summary describing the spatial distribution of ice for each year. Further, they could form the basis for interannual comparison by relating the spatial distributions of each end member. To test this application, the four end members developed previously were assumed to represent long-term general ice conditions* and were applied to the temporal sequences for 2 separate years, 1979 and 1984. These years were chosen to examine the capabilities of this approach in handling temporal sequences that differ considerably from the long-term mean because previous analyses have shown that 1979 was particularly icy in many parts of the Arctic, whereas teleconnections from the 1983 El Niño event were observed as abnormally low ice concentrations in 1984 (Piwowar and LeDrew, 1996).

Figure 7 compares temporal mixture and RMS error images for 1984, 1979, and the long-term average. Because the same long-term endmember set was used for each analysis, regions that have high errors in the error images are locations of significant deviation from the climate normal. The temporal characteristics of the anomalies are interpreted by analyzing the differences in color mixtures in the temporal mixture images. Several examples will demonstrate this technique.

The central core of nonseasonal sea ice took on a more elongated shape in 1979, extending farther into the Canadian Archipelago and abutting the Siberian coastline. In contrast, the ice along the Alaskan margins of the Beaufort Sea exhibit nonseasonal characteristics in 1984, indicating that high concentrations of ice remained in this area throughout the year. This phenomenon is part of a well-known reciprocation of the entire Arctic Ocean ice pack across the pole between the North American and Eurasian continents (Gloersen et al., 1993; Piwowar and LeDrew, 1996; Walsh and Johnson, 1979).

"Purer" colors in the Laptev, Kara, Barents, and Greenland Seas in the 1979 image indicate that higher end-member fractions were derived for this year than for the long-term average. This means that these regions fit their corresponding temporal spectra more closely than average, suggesting an increased presence of ice during the winter of 1979 or less ice in the summer of that year.

The Sea of Okhotsk had an unusually long and broad ice cover during 1979 and almost no ice at all in 1984. In fact, the 1979 fraction image for the third seasonal ice end member (shown in blue in Fig. 7 and in isolation in Fig. 8) had a fraction overflow for a significant part of this region, indicating the presence of temporal spectra that were purer than the end-member definition. To examine the nature of this condition, additional spectra were extracted for the overflow areas and compared with the end-member definition (Fig. 8). All of the sampled spectra show higher ice concentrations than does the modeled end member for the first 3 months of 1979. The same condition exists for the Bering Sea during 1984. During the preliminary end-member definition stage of SMA, fraction overflows are usually considered to represent error and are eliminated by redefining the end member. For interannual comparisons during TMA, however, fraction overflows are desirable because they assist in the quick identification of anomalous or changed conditions.

A unique attribute of temporal mixture images lies in their ability to summarize the mixing interactions between the pure end-member spectra. By knowing (or being able to determine) color definitions based on mixtures of red, green, and blue, one can estimate the relative proportion that each fraction is contributing to a given area simply by noting its color. For example, the brown color mixture along the Beaufort Sea coast of North America in the 1979 image does not appear elsewhere in these images. It is representative of a mixture of approximately 65% nonseasonal ice, 25% seasonal sea ice with temporal characteristics of the first seasonal end member, and 10% seasonal ice matching the second seasonal end member and contrasts with the long-term average where the first seasonal end member dominates. A review of the end-member spectra in Figure 4 for the brown areas in the 1979 image reveals that they would have been totally ice covered from November through May, with a large proportion remaining solidly covered throughout

*Ideally, end members derived over a 30-year data interval would have more climatic significance.

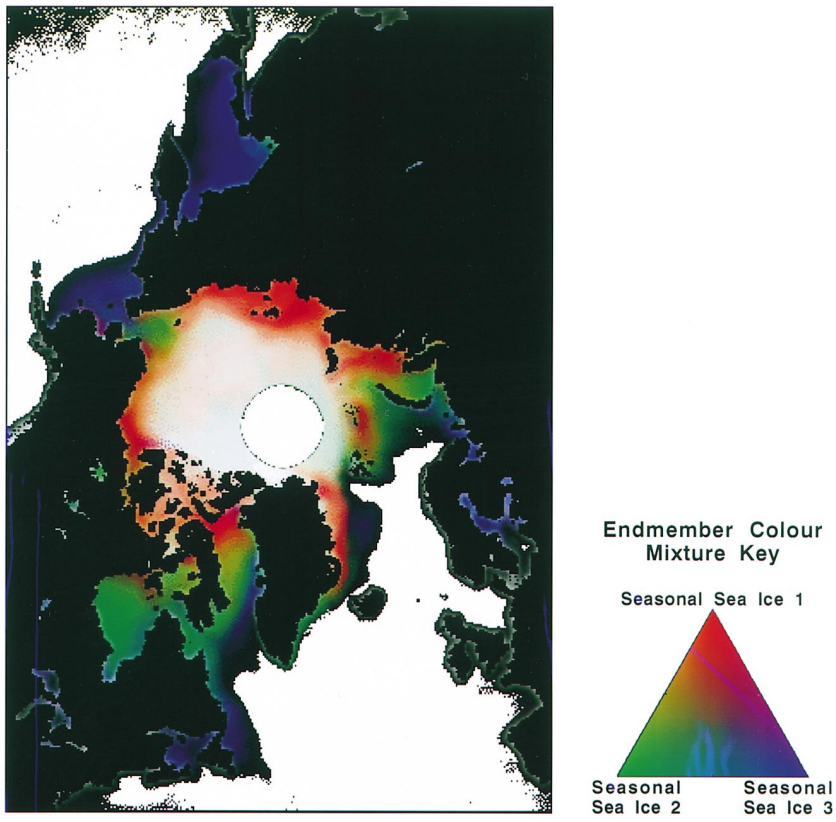

Figure 6. Temporal mixture image of 9-year average sea ice concentrations: a composite summary of the temporal characteristics of Arctic sea ice created by portraying the first seasonal fraction image in red, the second in green, and the third in blue. The nonseasonal sea ice fraction is shown in white. The "pureness" and intensity of each end member's color is directly related to the fractional contribution that each end member makes to the temporal characteristics of Arctic sea ice.

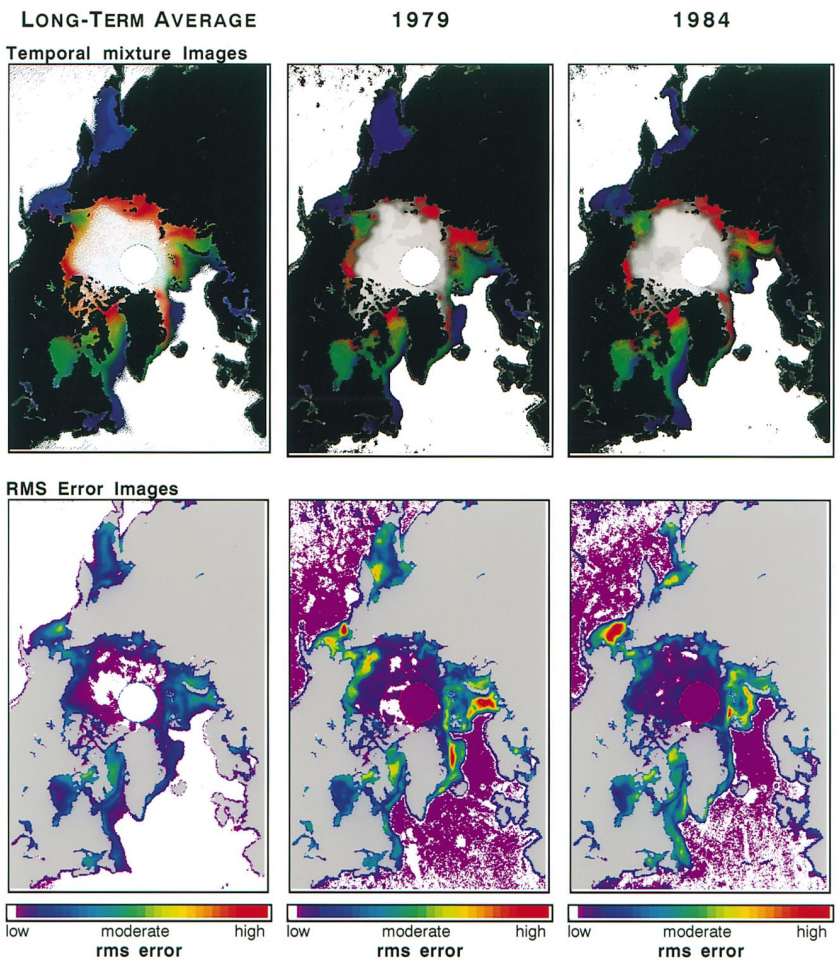

Figure 7. Temporal mixture and RMS error images for the long-term average, 1979, and 1984.

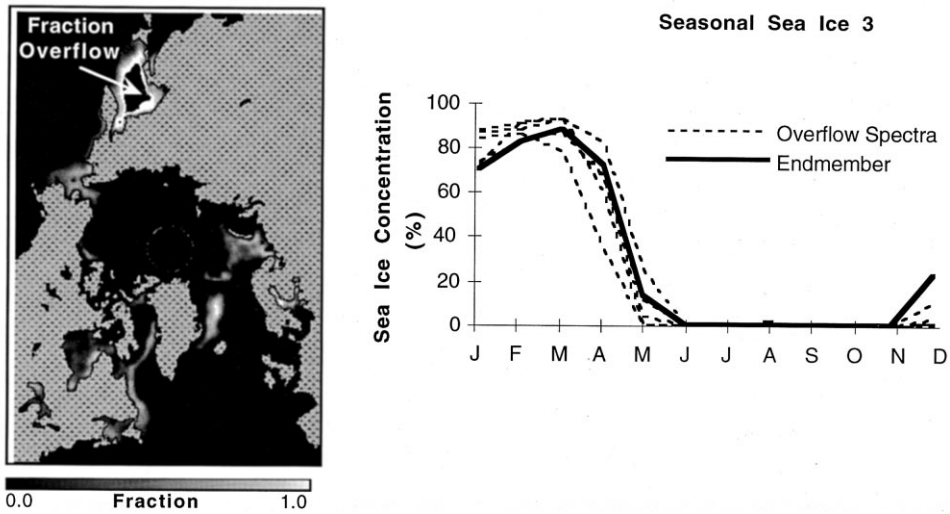

Figure 8. Fraction overflow in the Sea of Okhotsk for seasonal sea ice end-member 3 in 1979.

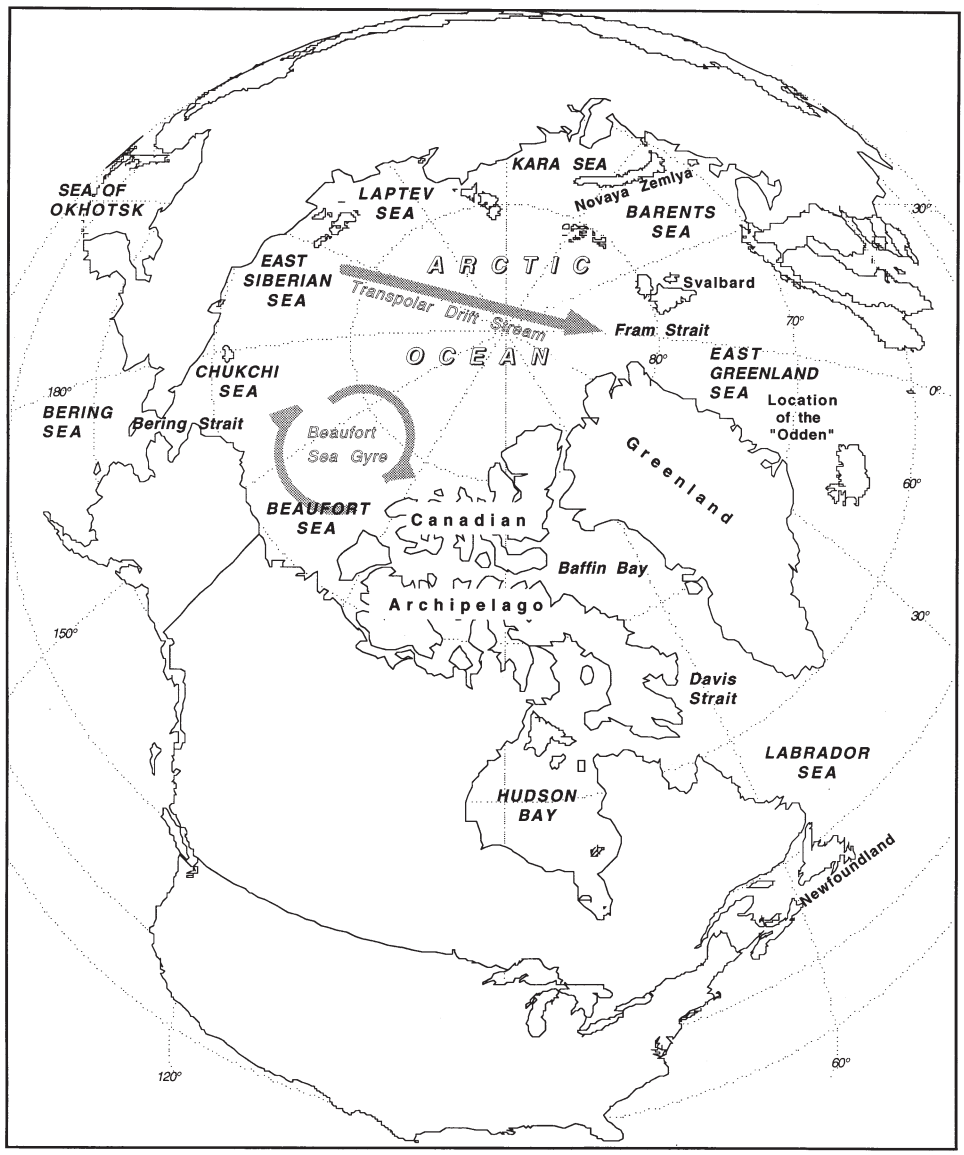

Figure 9. Arctic place-name reference map.

the year. About one-third of the area would have opened up for a brief summer in August and September.

OTHER ANALYSIS POSSIBILITIES

In this study, we unmixed temporal fractions from a 12-image summary from 9 years of SMMR imagery to represent a long-term normal. Another approach to analyzing change in the image sequence could be to use spectra from all of the 108 monthly images over the 9 years. The end members thus defined would represent various degrees of change in different parts of the temporal sequence. An examination of loadings plots from a principal components analysis of the same data may assist in defining the first few end members.

As mentioned earlier, the 9-year period examined was not long enough to attach any climatic significance to the changes observed (although it was sufficient to reveal large anomalies, such as those present during the El Niño years). The SMMR data set was chosen for this study to develop and evaluate the TMA procedure. The 9 SMMR years are only one part of a continuum of passive microwave imagery extending from 1973 to the present. We should soon be in a position where we can temporally unmix data from the entire time period to define a climatically significant long-term normal, if there can be a coherent ice concentration transformation between the different data sets. This will be the subject of a future communication.

Temporal mixture analysis is not necessarily restricted to passive microwave image data or sea ice applications. Terrestrial images from the NOAA advanced very high resolution radiometer (AVHRR) sensor are frequently used for climate change analyses because of their high temporal resolution (the satellite makes more than one pass each day, helping to ensure adequate data); medium spatial resolution (approximately 1 km at nadir, which is detailed enough for monitoring many environmental systems while minimizing unnecessary data volume); and historical data record (since 1978). For monitoring vegetation changes, AVHRR data can be composited into NDVI images that not only emphasize vegetative biomass, but also serve to satisfy the first and third hypertemporal data set requirements discussed earlier.

TMA could also be applied to higher spatial and temporal resolution data, such as airborne hyperspectral imagery, where it has the potential to reveal subtle patterns of diurnal or interseasonal variability.

SUMMARY AND CONCLUSIONS

In this study, the method of spectral mixture analysis has been extended and reinterpreted for use in the time domain and applied to a time series analysis of Arctic sea ice concentrations derived from remotely sensed imagery. This method, which we call temporal mixture analysis (TMA), has provided a new framework within which longer-term trends in sea ice change have been quantified and related to observed physical properties over time. For example, we found that the annual cycle of sea ice concentrations over the 9-year period studied for the entire Arctic can be modeled with four temporal end members created from theoretical and empirical derivations.

We also develop the concept of temporal mixture images. These images provide a unique summary of the spatial arrangement of the temporal characteristics of the mapped phenomenon during a specific period. A key distinction that differentiates temporal mixture imagery from similar images derived through other means (e.g., principal components analysis or image classification) is that the data presented are derived from the *temporal* characteristics of the analyzed phenomenon and not the *type* of feature present. For example, a region that is highlighted by a nonseasonal ice end member is not necessarily dominated by multiyear ice. It is, however, dominated by ice whose month-to-month variation is closely aligned with the temporal spectrum defined for this end member. End members refer to extreme—not average—conditions; real locations exhibiting these characteristics may or may not exist. These extreme conditions may serve as useful guides for engineering or climate modeling applications.

"Pure" spectra, in the context of spectral mixture analysis, means that, at any spectral interval, there should not be any other spectral samples with more extreme values than that of the end member. This concept was embodied in an empirically based purification formula developed in this study to derive pure end-member spectra from a sampled set of image spectra. The purification formula defines an end-member spectral value to be the most extreme (either maximum or minimum, depending on the context) sampled value at that period.

Our TMA also revealed an interesting phenomenon about the temporal character of Arctic sea ice concentrations: regions tend to remain generally ice free or ice covered during the year, suggesting that there are forces at work that cause sea ice to resist a change of state (freezing or thawing) well beyond the point at which atmospheric conditions indicate.

TMA was shown to be an effective tool for identifying changes between groups of temporal sequences (e.g., 1-year time series) and a reference sequence (e.g., a long-term normal). Fractional images summarize the temporal processes operating during a specific time period (e.g., 1 year) and could also serve as a historical record or summary describing the spatial and temporal characteristics of the analyzed phenomenon. The elegance of this solution should be of interest to creators of general circulation models, many of which treat the Arctic as a seasonally invariant slab of ice.

We have demonstrated the utility of TMA with the use of SMMR images of sea ice concentration. We see

great promise in the applicability of the technique for monitoring changes in more terrestrial features (such as the boreal forest) with the use of other sensor data (such as the NOAA AVHRR).

Financial support from the Natural Science and Engineering Research Council and the Institute for Space and Terrestrial Science is acknowledged. The SMMR ice concentration data set compiled by NASA/Goddard and distributed by the National Snow and Ice Data Center in Boulder, CO, is a wonderful resource to work with.

REFERENCES

Adams, J. B., Smith, Milton O., and Gillespie, Alan R. (1989), Simple models for complex natural surfaces: a strategy for the hyperspectral era of remote sensing. In *Proceedings of IGARSS'89/12th Canadian Symposium on Remote Sensing,* Vancouver, BC, Canada, Vol. 1, pp. 16–21.

Adams, J. B., Smith, M. O., and Gillespie, A. R. (1993), Imaging spectroscopy: interpretation based on spectral mixture analysis. In *Remote Geochemical Analysis: Elemental and Mineralogical Composition* (C. M. Pieters and P. Englert, Eds.), LPI and Cambridge University Press, Cambridge, Chap. 7.

Boardman, J. W. (1989), Inversion of imaging spectrometry data using singular value decomposition. In *Proceedings of IGARSS'89/12th Canadian Symposium on Remote Sensing,* Vancouver, BC, Vol. 4, pp. 2069–2072.

Comiso, J. C. (1986), Characteristics of Arctic winter sea ice from satellite multispectral microwave observations. *J. Geophys. Res.* 91:975–994.

Cross, A. M., Settle, J. J., Drake, N. A., and Paivinen, R. T. M. (1991), Subpixel measurement of tropical forest cover using AVHRR data. *Int. J. Remote Sens.* 12:1119–1129.

Davis, F. W., Quattrochi, D. A., Ridd, M. K., Lam, N. S., Walsh, S. J., Michaelsen, J. C., Franklin, J., Stow, D. A., Johannsen, C. J., and Johnston, C. A. (1991), Environmental analysis using integrated GIS and remotely sensed data: some research needs and priorities. *Photogramm. Eng. Remote Sens.* 57:689–697.

Eastman, J. R., and Fulk, M. (1993), Long sequence time series evaluation using standardized principal components. *Photogramm. Eng. Remote Sens.* 59:1307–1312.

Gillespie, A. R., Smith, M. O., Adams, J. B., and Willis, S. C. (1990), Spectral mixture analysis of multispectral thermal infrared images. In *Proceedings of the Second Thermal IR Multispectral Scanner (TIMS) Workshop,* JPL Publication No. 90-55, 57–74.

Gloersen, P., Campbell, W. J., Cavalieri, D. J., Comiso, J. C., Parkinson, C. L., and Zwally, H. J. (1993), *Arctic and Antarctic Sea Ice, 1978–1987: Satellite Passive-Microwave Observations and Analysis.* National Aeronautics and Space Administration, Washington, DC, NASA SP-511.

Gong, P., Miller, J. R., Freemantle, J., and Chen, B. (1991), Spectral decomposition of Landsat thematic mapper data for urban land-cover mapping. In *Proceedings of 14th Canadian Symposium on Remote Sensing,* Calgary, Alberta, pp. 458–461.

Hall, F. G., Shimabukuro, Y. E., and Huemmrich, K. F. (1995), Remote sensing of forest biophysical structure in boreal stands of *Picea mariana* using mixture decomposition and geometric reflectance models. *Ecol. Appl.* 5:993–1013.

Hoffbeck, J. P., and Landgrebe, D. A. (1993), Classification of high dimensional multispectral image data. In *Proceedings of Fourth Annual JPL Airborne Geoscience Symposium,* Washington, DC, 25–29 Oct.

Horwitz, H. M., Nalepka, R. F., Hyde, P. D., and Morgenstern, J. P. (1971), Estimating the proportions of objects within a single resolution element of a multispectral scanner. In *Proceedings of Seventh International Symposium on Remote Sensing of Environment,* ERIM, Vol. 2, pp. 1307–1320, 17–21 May.

LeDrew, E. (1992), The role of remote sensing in the study of atmosphere-cryosphere interactions in the polar basin. *Can. Geogr.* 36:336–350.

PCI (1996), *PACE Neural Network Reference Manual.* PCI Inc., Richmond Hill, Ontario, Canada.

Peddle, D. R., LeDrew, E. F., and Holden, H. M. (1995), Spectral mixture analysis of coral reef abundance from satellite imagery and *in situ* ocean spectra, Savusavu Bay, Fiji. *Proceedings Third Thematic Conference on Remote Sensing for Marine and Coastal Environments,* Vol. 2, pp. 563–575, 18–20 September 1995, Seattle, WA.

Peddle, D. R., Hall, F. G., and LeDrew, E. F. (in press), Spectral mixture analysis and geometric optical reflectance modeling of boreal forest biophysical structure. *Remote Sens. Environ.*

Piwowar, J. M., and LeDrew, E. F. (1996), Principal components analysis of Arctic ice conditions between 1978 and 1987 as observed from the SMMR data record. *Can. J. Remote Sens.* 22:390–403.

Sabol, D. E., Jr., Adams, J. B., and Smith, M. O. (1990), Predicting the spectral detectability of surface materials using spectral mixture analysis. In *Proceedings of IGARSS'90,* pp. 967–970, 20–24 May, 1990, Washington, DC.

UCAR (1990), *Recommendations from an interdisciplinary forum on data management for global change.* UCAR Report No. OIES-5, Boulder, CO.

Unger, S. G., and Bryant, E. (1981), Fanning: a classification algorithm for mixture landscapes applied to Landsat data of Maine forests. In *Proceedings of 15th International Symposium on Remote Sensing of Environment,* pp. 1113–1120.

Ustin, S. L., Smith, M. O., and Adams, J. B. (1993), Remote sensing of ecological processes: a strategy for developing and testing ecological models using spectral mixture analysis. In *Scaling Physiological Processes: Leaf to Globe* (J. R. Ehleringer and C. B. Field, Eds.), Academic Press, San Diego, pp. 339–357.

Walsh, J. E., and Johnson, C. M. (1979), An analysis of Arctic sea ice fluctuations, 1953-77. *J. Phys. Oceanogr.* 9:580–591.